Design Study of a Small Scale Soft Recovery System

Ilyong Yoo
Ph.D. Student, Department of Aerospace Engineering, Inha University, Incheon 402-751, Korea
Seungsoo Lee*
Department of Aerospace Engineering, Inha University, Incheon 402-751, Korea
Chongdu Cho
Department of Mechanical Engineering, Inha University, Incheon 402-751, Korea

A soft recovery system (SRS) is a device that stops a high speed projectile without damaging the projectile. The SRS is necessary to verify the shock resistant requirements of microelectronics and electro-optic sensors in smart munitions, where the projectiles experience over 20,000 g acceleration inside the barrel. In this study, a computer code for the performance evaluation of a SRS based on ballistic compression decelerator concept has been developed. It consists of a time accurate compressible one-dimensional Euler code with use of deforming grid and a projectile motion analysis code. The Euler code employs Roe's approximate Riemann solver with a total variation diminishing (TVD) method. A fully implicit dual time stepping method is used to advance the solution in time. In addition, the geometric conservation law (GCL) is applied to predict the solutions accurately on the deforming mesh. The equation of motion for the projectile is solved with the four-stage Runge-Kutta time integration method. A small scale SRS to catch a 20 mm bullet fired at 500 m/s within 1,600 g-limit has been designed with the proposed method.

Key Words : Smart Munitions, SRS (Soft Recovery System), Ballistic Compression Decelerator, Roe's Approximate Riemann Solver, Dual Time Stepping Method, GCL (Geometric Conservation Law)

Nomenclature

$\mathbf{A}$: Jacobian matrix
$\mathbf{E}$: Flux vector
$\hat{\mathbf{E}}$: Numerical flux
$\bar{\mathbf{E}}$: Generalized flux
$\mathbf{I}$: Identity matrix
$\mathbf{Q}$: Solution vector
$\mathbf{R}$: Residual vector
L_1, L_2, L_3 : High pressure tube lengths
P_1, P_2, P_3 : Initial tube pressures
V_p : Velocity of projectile
X_p : Projectile stop distance
a_p : Maximum deceleration Rate
b : Covolume constant
c : Speed of sound
$\bar{c}$: Equivalent speed of sound
d : Projectile diameter
e : Total energy
k : Relative velocity to cell surface
$h=\frac{p+e}{\rho}$: Enthalpy
p : Pressure
u : Velocity
t : Time

* Corresponding Author,
E-mail : slee@inha.ac.kr
TEL : +82-32-860-7358; **FAX** : +82-32-865-5401
Department of Aerospace Engineering, Inha University, Incheon 402-751, Korea. (Manuscript **Received** February 21, 2006; **Revised** August 24, 2006)

Δt : Time increment
L : Cell length
M : Projectile mass

Greek letters

ρ : Density
ξ_t : Grid velocity
γ : Ratio of specific heats
λ : Eigenvalue of jacobian matrix
ϕ, θ : Parameters of time stepping method
τ : Fictitious time
Γ : Equivalent ratio of specific heats
Δ : Correction

Superscripts

n : Real time level
l : Fictitious time level

Subscripts

i : Cell index
R : Right state
L : Left state

1. Introduction

With the advances in electro-optic sensors and piezoelectric actuators, smart projectiles become a reality. Since the acceleration experienced by the projectile inside a gun barrel could exceed 20,000 g, sensitive sensors or actuators might be damaged during fire. For post-firing diagnostics of the sensor and the projectile itself, we need to stop the projectiles without damaging the projectiles or the sensors during the recovery process. Soft recovery system (SRS) is defined as a device that stops projectiles within a given deceleration limit. In addition, it is required that the projectile should be fired from a standard form of gun barrel with a standard propellant charge and that the projectile should not be modified in any way. The deceleration limit is set by the system specification of sensors or actuators, and is usually one order of magnitude less than the acceleration during fire.

There exist several forms of SRS (Clarke et al., 1981 ; Evans et al., 1981 ; Hölzle, 2001 ; Teng, 1972). The primitive form of SRS is firing projectiles vertically and allowing them to fall back into a plowed dirt recovery field. Using costal waters as recovery medium is another simple method. With these approaches, however, the linear deceleration of the projectiles cannot be controlled. Army Research Laboratory (ARL) had constructed a Large Caliber Soft Recovery System (LCSRS) (Clarke et al., 1981 ; Evans et al., 1981), which used water as recovery medium. Soft recovery was achieved by attaching a water scoop to the projectile and firing it into an open water channel inclined at a small angle. The deceleration rate can be controlled by changing the inclination angle of the water channel. One of main advantages of the system is that it is applicable to different caliber projectiles by changing the gun barrel attached to the system. However, the projectile had to be modified to accommodate the water scoop. Hölzle (2001) proposed an SRS that consisted of two 60 m containers filled with about 30 tons of rubber granules. A thick plate was used to soften the initial impact when the projectile entered the system. This system, however, cannot be used for spin stabilizing projectiles. Furthermore, the initial impact is so high that the projectile might be damaged during the recovery.

A physically sound concept of soft recovery is the ballistic compression decelerator proposed by Teng (1972). An SRS of this type was built by a German company Rheinmetall W&M and is being operated successfully over the years. This system can catch an 840 m/s 155 mm projectile in 200 m. They suggested that the projectile be fired into a series of pre-pressurized tubes known as decelerator tubes that are separated by diaphragms. A shock preceded by the projectile ruptures the diaphragms before entering the decelerator tubes. The ballistic compression decelerator can be thought of as shock tubes connected in serial. From the interactions of shocks and rarefaction waves, the pressure builds up ahead of the projectile to slow it down. By changing the number, the lengths and the initial pressures of the tubes or the type of the gas filled inside the tubes, we can control the deceleration rates as desired. There is no need to modify the projectile to be used in the system. One of the disadvantages is that it uses long tubes and multiple diaphragms. Therefore, it is expensive to construct and it occupies a large amount of real

estates. Also, debris from rupturing the diaphragms might damage the projectiles.

In this paper, we present a performance analysis method for the SRS based on the concept of the ballistic compression decelerator. This paper is organized as follows. In Section 2, we will discuss the physical process involved in the SRS in detail. In Section 3, the geometric and mathematical models will be discussed. In Section 4, we will present a design result of a small scale SRS for capturing a 20 mm bullet fired at 500 m/s within a deceleration limit of 1,600 g.

2. Ballistic Compression Decelerator

Figure 1(a) depicts the schematic of the SRS based on the ballistic compression decelerator concept. The ballistic compression decelerator is a long tube attached to a gun barrel. The tube whose diameter is the same as projectile's diameter is divided into a series of the decelerator tubes. The decelerator tubes are separated by diaphragms that will be broken if the pressure difference exceeds the design rupture pressure. Each decelerator tubes are pressurized initially with air or other working gases. After the projectile launched, it passes through muzzle breaker that relieves the launch gases. Thus, it can be assumed that the base pressure of the projectile is atmospheric. Also, we ignore the friction between the projectile and the tubes. After fire, a shock forms ahead of the projectile, and travels faster than the projectile as shown in Fig. 1(b). The shock and the reflected shock on the diaphragm compress air near the diaphragm to even higher pressure than the next decelerator tube. The diaphragm raptures because the pressure difference is higher than the diaphragm rupture pressure. The shock traveling through relatively low-pressure region arrives at the next diaphragm. And the whole processes repeat. The number of high-pressure tubes, the lengths, and the initial pressures of the tubes are the design variables of the SRS.

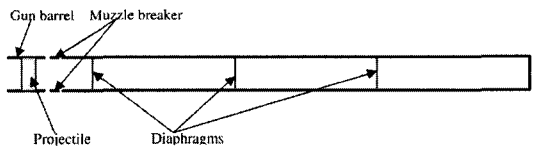

(a) Schematic of soft recovery system

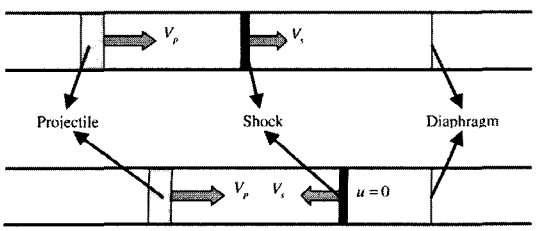

(b) Shock reflection on the Diaphragm

Fig. 1 Ballistic compression decelerator

3. Performance Analysis Method for SRS

3.1 Flow solver

In order to simulate the flow inside the SRS more realistically, the state of the gas inside the SRS is assumed to obey the covolume equation of state. Furthermore, the flow is assumed to be one-dimensional and inviscid, which of course neglects heat transfer to the tube wall. The assumption on one dimensionality can be justified by the fact that the ratio of the length to the diameter of a typical SRS is over 100. Figure 2 shows a one-dimensional moving and deforming grid system inside the SRS. Domain between the head of the projectile and the diaphragm is discretized by dividing the domain into a number of cells. As the projectile moves, the grid deforms as shown in Fig. 2. The deformation of the grid can be done easily by simple shearing. After the diaphragm ruptures, the region inside the next tube is also discretized. The diaphragm is assumed to be broken when the pressure difference of the diaphragm exceeds the designed rupture pressure. The one-dimensional compressible Euler code is applied on the computational grid to obtain the pressure at the head of the projectile. As stated earlier, the motion of the projectile is assumed to be frictionless. Moreover, it is assumed that there is no pressure leak through the projectile. The pressure difference on both side of the projectile determines the motion of the projectile. After a complete stop, furthermore, the static friction between the

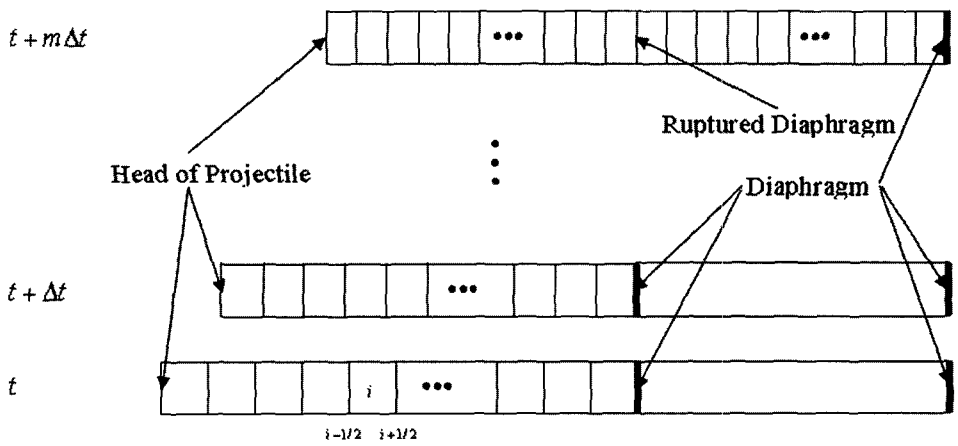

Fig. 2 Moving and deforming grid system

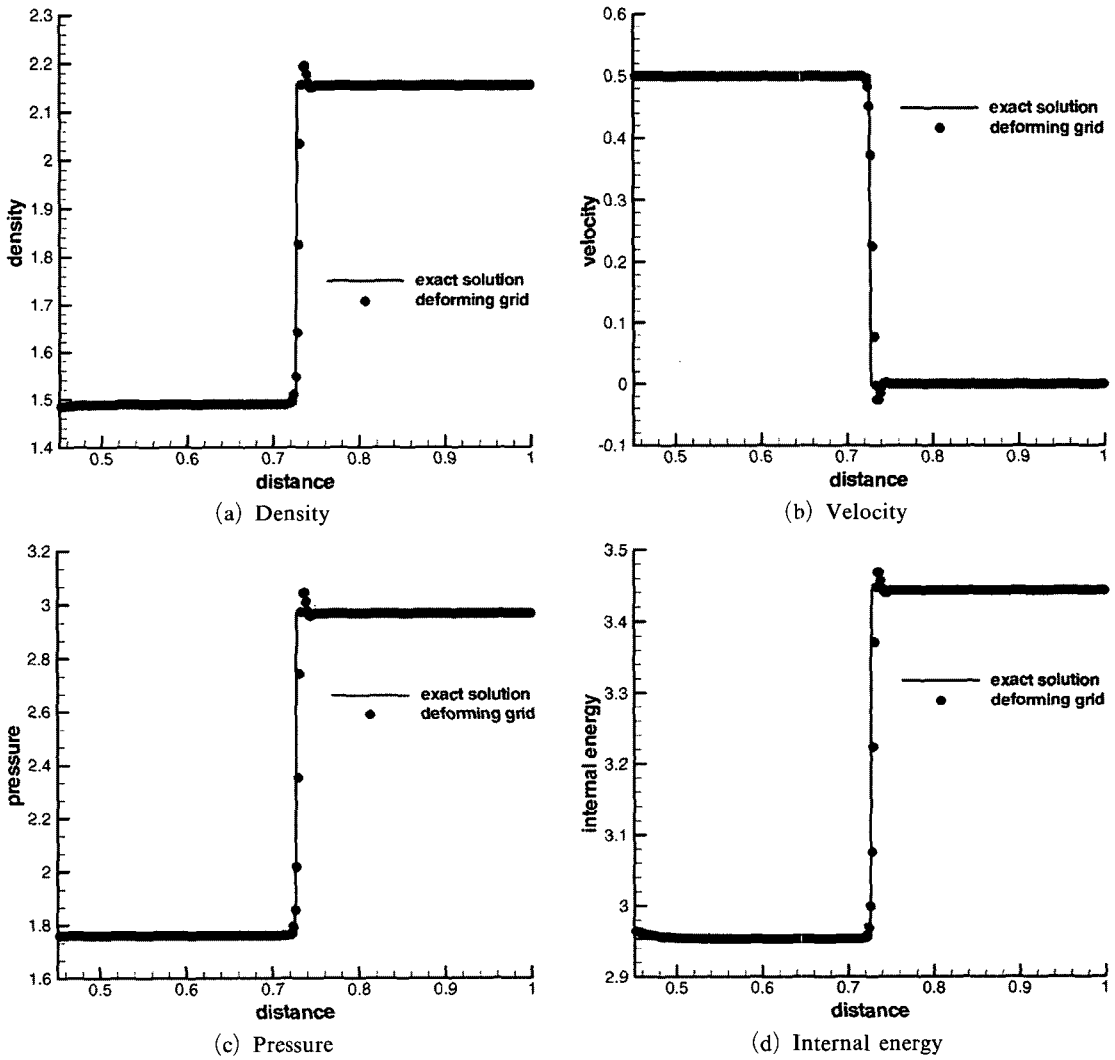

(a) Density (b) Velocity

(c) Pressure (d) Internal energy

Fig. 3 Comparison of numerical solutions with moving grid and deforming grid : Moving shock problem

projectile and the SRS wall is assumed to keep the projectile where it stops.

The one-dimensional compressible Euler equation can be written as

$$\frac{\partial \mathbf{Q}}{\partial t}+\frac{\partial \mathbf{E}}{\partial x}=0 \tag{1}$$

The solution vector and the flux vector are defined by

$$\mathbf{Q}=\begin{bmatrix}\rho\\ \rho u\\ e\end{bmatrix},\ \mathbf{E}=\begin{bmatrix}\rho u\\ \rho u^2+p\\ (e+p)u\end{bmatrix} \tag{2}$$

where ρ, u, and e are the density, the velocity and the total energy of the gas. The pressure can be evaluated from the equation of state for the covolume gas.

$$p=(\gamma-1)(1-b\rho)\left(e-\rho\frac{u^2}{2}\right) \tag{3}$$

where b is the covolume constant. In this paper, we use $b=0.001\ \mathrm{m^3/kg}$ (Baysal, 1986).

If we integrating Eq. (1) over a deforming grid depicted in Fig. 3, and apply the Reynolds transport theorem, we have

$$\frac{d}{dt}(L\mathbf{Q})+\hat{\mathbf{E}}_{i+1/2}-\hat{\mathbf{E}}_{i-1/2}=0 \tag{4}$$

where L is the length of the cell i. Here, the generalized flux is defined by

$$\hat{\mathbf{E}}=\begin{bmatrix}\rho k\\ \rho u k+p\\ (e+p)k+p\xi_t\end{bmatrix} \tag{5}$$

where $k=u-\xi_t$ is the relative velocity to the cell surface and ξ_t is the grid velocity. For stable computations, we replace the generalized flux vector with Grossman and Walter's version of Roe's numerical flux for real gas (Grossman and Walters, 1989) for moving grid

$$\tilde{\mathbf{E}}_{i+1/2}=\frac{1}{2}[\hat{\mathbf{E}}(\mathbf{Q}_R)+\hat{\mathbf{E}}(\mathbf{Q}_L)-|\mathbf{A}|(\mathbf{Q}_R-\mathbf{Q}_L)] \tag{6}$$

where $\mathbf{A}$ is the Jacobian matrix of the generalized flux vector $\hat{\mathbf{E}}$. MUSCL extrapolation (Van Leer, 1979) for $\mathbf{Q}_L$ and $\mathbf{Q}_R$ is used for higher spatial accuracy. We use Van Albada's limiter to maintain TVD (Total Variation Diminishing) property near sharp solution gradient region. The dissipation term of Eq. (6) can be written compactly as

$$\begin{aligned}|\mathbf{A}|(\mathbf{Q}_R-\mathbf{Q}_L)=&\left(\delta\rho-\frac{\delta p}{\bar{c}^2}\right)|k|\begin{bmatrix}1\\ u\\ u^2/2\end{bmatrix}\\ &+\frac{\rho}{2\bar{c}}\left(\frac{\delta p}{\rho\bar{c}}+\delta u\right)|k+\bar{c}|\begin{bmatrix}1\\ u+\bar{c}\\ h+u\bar{c}\end{bmatrix}\\ &+\frac{\rho}{2\bar{c}}\left(\frac{\delta p}{\rho\bar{c}}-\delta u\right)|k-\bar{c}|\begin{bmatrix}1\\ u-\bar{c}\\ h-u\bar{c}\end{bmatrix}\end{aligned} \tag{7}$$

where the equivalent speed of sound and the speed of sound are defined by

$$\begin{aligned}\bar{c}^2&=\frac{(\bar{\gamma}-1)\Gamma}{\bar{\gamma}}\left(h-\frac{u^2}{2}\right),\\ c^2&=\frac{\gamma p}{\rho(1-b\rho)}=\frac{\Gamma p}{\rho}\end{aligned} \tag{8}$$

The values of $\rho, u, h, \bar{\gamma}$ and Γ at the cell interface in Eq. (7) are evaluated from Roe's average of the left and the right states. The eigenvalues $\lambda=k, k+\bar{c}$, and $k-\bar{c}$ appeared in Eq. (7) are modified to enforce the entropy condition following Harten (1983).

Equation (4) with the numerical flux can be written as

$$\frac{d}{dt}(L\mathbf{Q})+\mathbf{R}=0 \tag{9}$$

where the residual vector is defined by

$$\mathbf{R}=\tilde{\mathbf{E}}_{i+1/2}-\tilde{\mathbf{E}}_{i-1/2} \tag{10}$$

The two-parameter family of an A-stable two-step time integration method can be written as

$$\begin{aligned}&\left(1+\frac{\phi}{2}\right)\frac{\Delta(L\mathbf{Q})^n}{\Delta t}-\frac{\phi}{2}\frac{\Delta(L\mathbf{Q})^{n-1}}{\Delta t}\\ &+\theta\mathbf{R}^{n+1}+(1-\theta)\mathbf{R}^n=0\end{aligned} \tag{11}$$

where the correction, $\Delta(L\mathbf{Q})^n$ is defined by

$$\Delta(L\mathbf{Q})^n=(L\mathbf{Q})^{n+1}-(L\mathbf{Q})^n \tag{12}$$

The superscript n denotes the time integration

level. The values of ϕ and θ determine the spatial accuracy of the scheme.

$$\begin{aligned} \phi&=1 \quad : \text{2nd oder in time} \\ &=0 \quad : \text{1st oder in time} \\ \theta&=1 \quad : \text{Euler Implicit} \\ &=1/2 : \text{Trapezoidal Implicit} \\ &=0 \quad : \text{Euler Explicit} \end{aligned} \tag{13}$$

We used $\phi=1$, and $\theta=1/2$ throughout the paper. The dual time stepping (Merkle and Athavale, 1987) uses an inner fictitious time-step, in order to advance the unsteady equation in time. These inner iterations reduce the linearization error as well as the time-lag error associated with the explicit application of boundary conditions at the block interfaces and the diaphragm. Upon applying the dual time stepping method, we have

$$\left[\mathbf{D}+\theta\frac{\Delta\tau}{L}\left(\frac{\partial\mathbf{R}}{\partial\mathbf{Q}_{i+1}}+\frac{\partial\mathbf{R}}{\partial\mathbf{Q}_i}+\frac{\partial\mathbf{R}}{\partial\mathbf{Q}_{i-1}}\right)\right]\Delta\mathbf{Q}^l = -\Delta\tau\tilde{\mathbf{R}} \tag{14}$$

where

$$\mathbf{D}=\left\{\left(1+\frac{\phi}{2}\right)\frac{\Delta\tau}{\Delta t}+1\right\}\mathbf{I} \tag{15}$$

$$\tilde{\mathbf{R}}=\frac{1}{L^{n+1}}\left[\left(1+\frac{\phi}{2}\right)\frac{L^{n+1}\mathbf{Q}^l-(L\mathbf{Q})^n}{\Delta t} -\frac{\phi}{2}\frac{\Delta(L\mathbf{Q})^{n-1}}{\Delta t}+\theta\mathrm{R}^l+(1-\theta)\mathbf{R}^n\right] \tag{16}$$

$$\Delta\mathbf{Q}^l=\mathbf{Q}^{l+1}-\mathbf{Q}^l \tag{17}$$

The superscript l denotes the fictitious time integration level. At convergence, $\mathbf{Q}^{n+1}=\mathbf{Q}^{l+1}=\mathbf{Q}^l$, Eq. (16) reduces to $\tilde{\mathbf{R}}=0$, or Eq. (11). The time increment Δt is determined for the solution accuracy, while the fictitious time increment $\Delta\tau$ is determined for the numerical stability. The Jacobian matrices of the residual vector are approximately given by

$$\frac{\partial\mathbf{R}}{\partial\mathbf{Q}_{i+1}}\simeq\frac{1}{2}\{\mathbf{A}_{i+1}-\rho(\mathbf{A}_{i+1/2})\mathbf{I}\} \tag{18}$$

$$\frac{\partial\mathbf{R}}{\partial\mathbf{Q}_i}\simeq\frac{1}{2}\{\rho(\mathbf{A}_{i+1/2})+\rho(\mathbf{A}_{i-1/2})\}\mathbf{I} \tag{19}$$

$$\frac{\partial\mathbf{R}}{\partial\mathbf{Q}_{i-1}}\simeq-\frac{1}{2}\{\mathbf{A}_{i+1}+\rho(\mathbf{A}_{i-1/2})\mathbf{I}\} \tag{20}$$

where $\rho(\mathbf{A})$ denotes the spectral density of the matrix $\mathbf{A}$.

It is required that $\mathbf{Q}(x,t)=$constant be the solution to the discretized equation, Eq. (11). It is well known that if we compute the cell size at a given time level with geometric consideration only, Eq. (11) cannot be satisfied exactly with a uniform flow (Thomas and Lombard, 1978). In order for the requirement to be satisfied, the cell size should be computed with the geometric conservation law, which can be derived by substituting $\mathbf{Q}=C$ into Eq. (11).

$$L^{n+1}=L^n+\frac{\phi}{2+\phi}(L^n-L^{n-1}) -\frac{2\Delta t}{2+\phi}\left[\theta(\xi_{t_{i+1/2}}-\xi_{t_{i-1/2}})^{n+1} +(1-\theta)(\xi_{t_{i+1/2}}-\xi_{t_{i-1/2}})^n\right] \tag{21}$$

3.2 Projectile motion

The equation of motion for the projectile is given by

$$M\frac{d^2x}{dt^2}=-\frac{\pi d^2}{4}(p_f-p_b) \tag{22}$$

where d is the diameter of the projectile, and p_f, p_b are the head, and the base pressure of the projectile respectively. As stated earlier, the base pressure p_b is assumed atmospheric. Equation (22) is solved using 4-stage Runge-Kutta method that is 4th order accurate in time.

3.3 Verification of flow analysis

As described earlier, the physical process involved in the SRS can be divided into moving piston problem, shock reflection problem and shock tube problem. We choose these three problems to verify our flow analysis code. We present the first validation problem, a moving piston problem. A piston moves into a stationary gas. A shock is formed ahead of the piston, and travels faster than the piston. The initial values for the density, the speed of sound and the pressure are normalized to 1. The speed of the piston is chosen to be $V_p=0.5$, which generates a shock moving at $V_s=1.521$. In this computation is done with the

covolume constant of $b=0$, which is equivalent to an ideal gas. Two computational grids are used for the computation : a moving grid, and a deforming grid. While both ends of the moving grid move rigidly with the piston, the one end of the deforming grid is held fixed so that the grid is shrinking as the piston moves. The numbers of grid points of the two grids are 301. In the Fig. 3, the distributions of the density, the velocity, the pressure and the internal energy at $t=0.3$ are presented. As can be seen in the figure, the computational results with both grid systems match well with the exact solution.

The shock reflection problem is a continuation of the moving shock problem. The right end of the boundary is a solid wall on which the moving shock reflects. In Fig. 4, the density, the velocity, the pressure and the internal energy are compared with the exact solution at $t=0.9$. Only the deforming grid is used in this computation. The computed speed of the reflected shock is $V_s=1.122$, while the exact shock speed is $V_s=1.121$.

The third test is known as Sod's problem (Sod, 1978). This problem is a standard benchmark test problem for the validation of compressible Euler codes. The density ratio and the pressure ratio of the left and the right state are 8 and 10, respectively. Two grids are used for the computation :

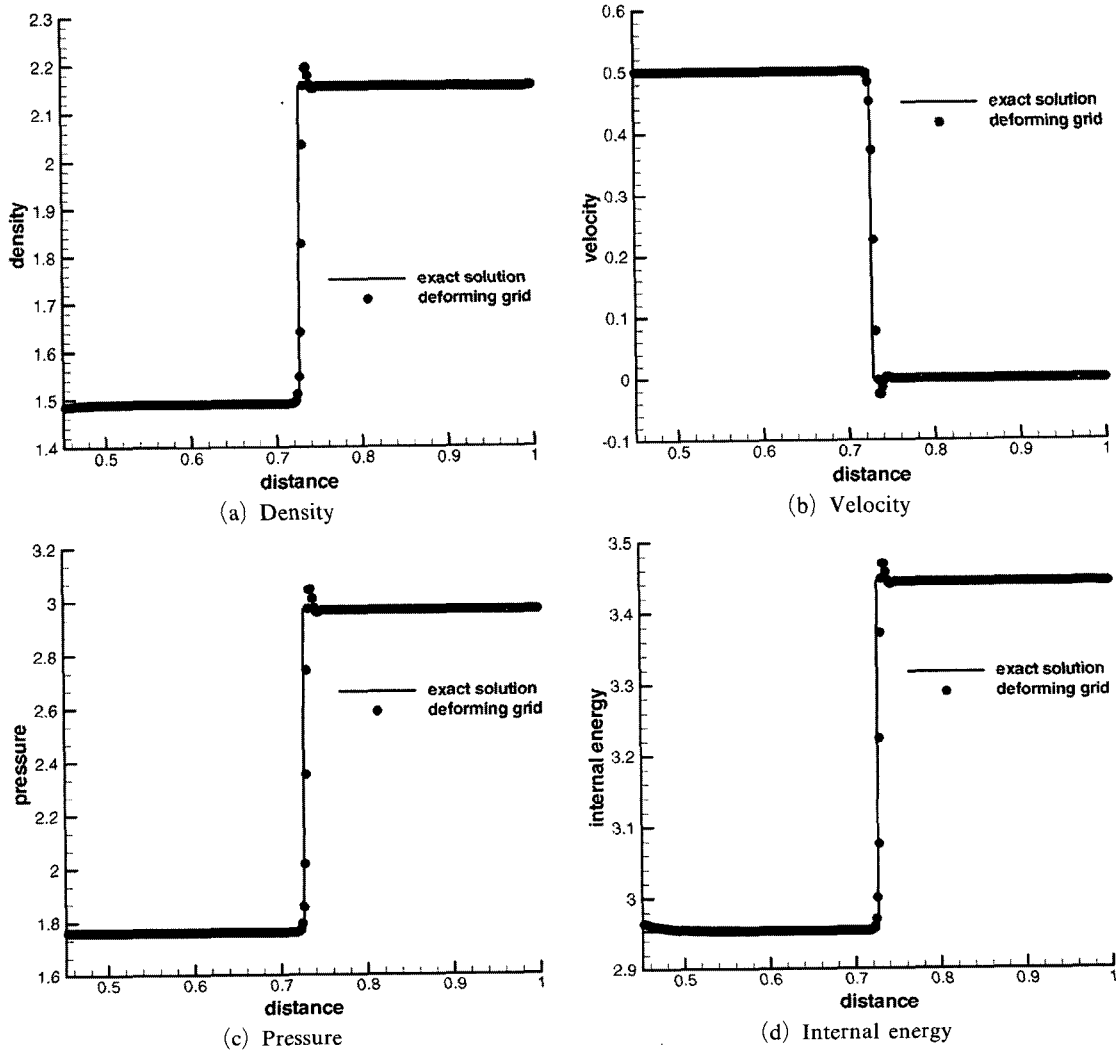

(a) Density (b) Velocity

(c) Pressure (d) Internal energy

Fig. 4 Comparison of numerical solutions with deforming grid : shock reflection problem

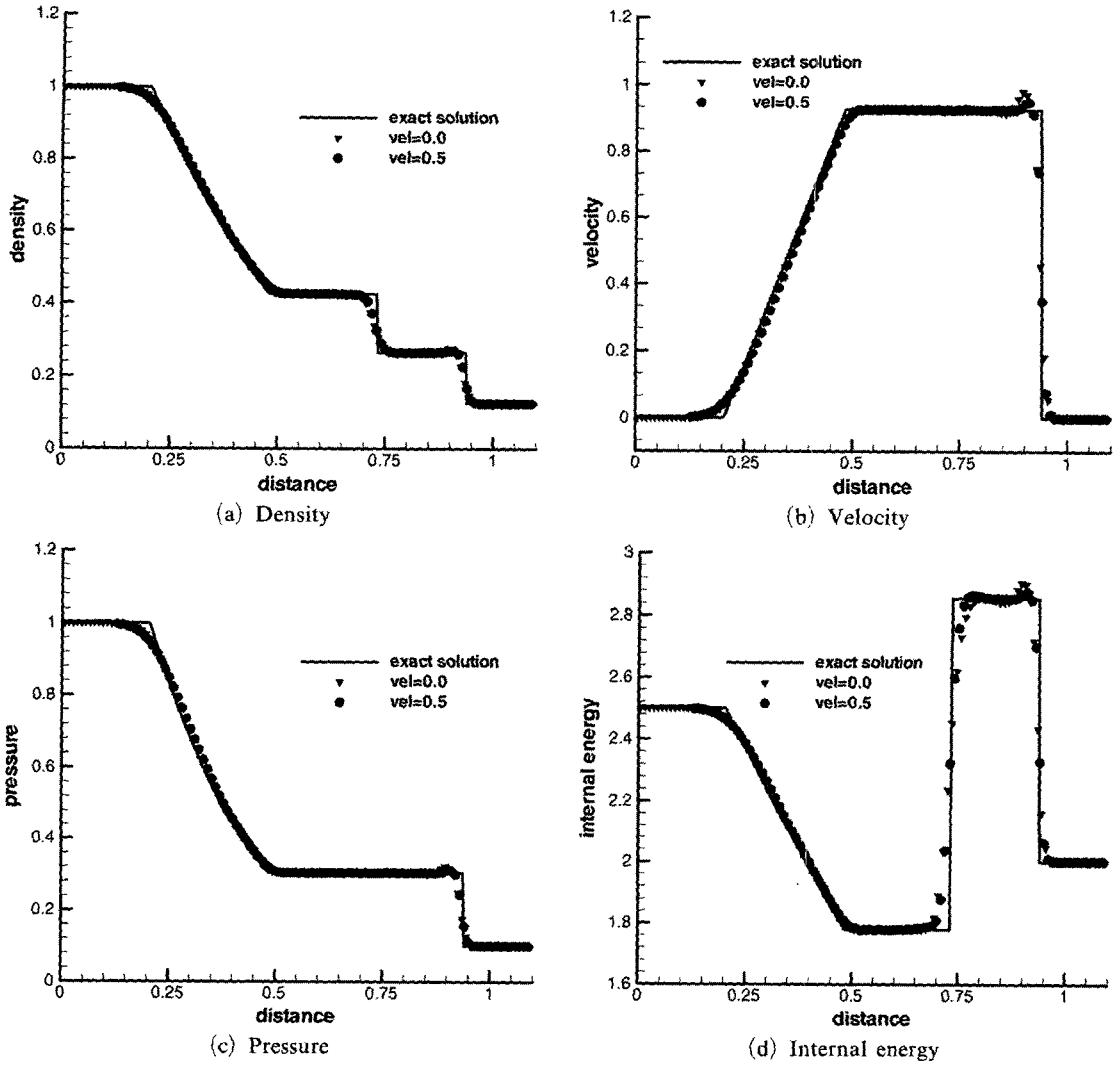

(a) Density (b) Velocity

(c) Pressure (d) Internal energy

Fig. 5 Comparison of numerical solutions with fixed grid and moving grid : Sod problem

the fixed grid and the moving grid. The velocity of moving grid is set to $\xi_t=0.5$. The numbers of the grid points for both grid systems are 101. The solutions are presented in Fig. 5 and compared with the exact solutions showing good agreement.

4. Design Results of Small Scale SRS

With the performance analysis code for the SRS, a small scale SRS capable of capturing a 20 mm bullet within a deceleration limit of 1,600 g has been designed. The initial velocity of the bullet is selected to be 500 m/s. In order to simplify the design process, the number of the decelerator tubes is set to 3. In addition, the length of the atmospheric tube ahead of the decelerator tubes is set to 1 m. As described earlier, the muzzle breaker located in this tube relieves the launch gases and the shock is formed first inside this tube. As a result, we have 6 design variables for the design of the small scale SRS. We will use the subscript to indicate the tubes. For example, P_1 and L_1 denote the initial pressure and the length of the first decelerator tube.

The design objectives are chosen to minimize not only the distance for the bullet to stop but

also the maximum pressure occurring inside the SRS while the deceleration kept under 1,600 g. The design variables are chosen as L_1=12 m, L_2=8 m, L_3=4 m, P_1=8 atm, P_2=15 atm and P_3=1 atm by surveying the design space. Figures 6 and 7 show the sensitivity of the stop distance, X_p and the maximum pressure, P_{max} as P_1 and P_2 vary. Other design variables are fixed at the designed values. In addition, the constant maximum deceleration contours, a_p are plotted on these figures. As P_1 increases, X_p decreases, but a_p and P_{max} increase. On the other hand, as P_2 increase, X_p reduces. However, change in P_2 has small influence on a_p and P_{max}. The maximum deceleration occurs when the shock reflected on the first diaphragm impinges on the bullet if $P_1>9$ atm and $P_2<18$ atm. Otherwise, the maximum deceleration occurs when the second reflected shock hits the bullet. Therefore, it is concluded that P_1=8 atm, P_2=15 atm would be a good choice to keep the deceleration rate within the limit and to keep the maximum pressure low. Figures 8 and 9 depict the design space in terms of L_1 and L_2. Other design variables are kept at their designed values. As can be seen from the plots, shortening L_2 increases the deceleration

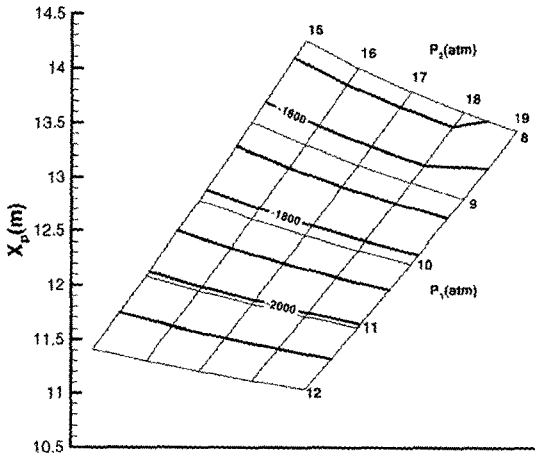

Fig. 6 Design space of SRS (X_p in terms of P_1 and P_2)

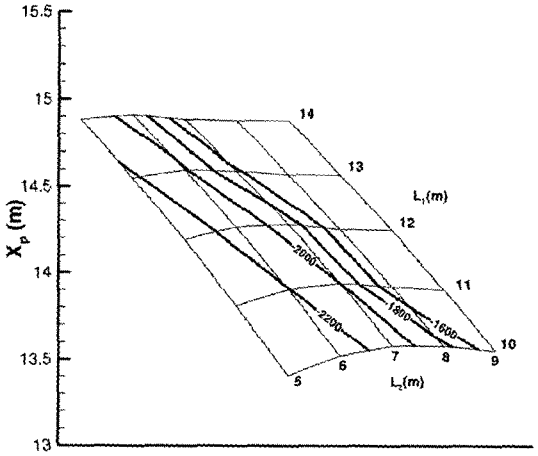

Fig. 8 Design space of SRS (X_p in terms of L_1 and L_2)

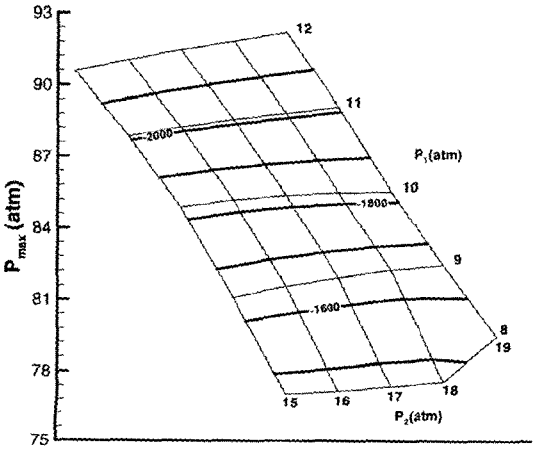

Fig. 7 Design space of SRS (Pmax in terms of P_1 and P_2)

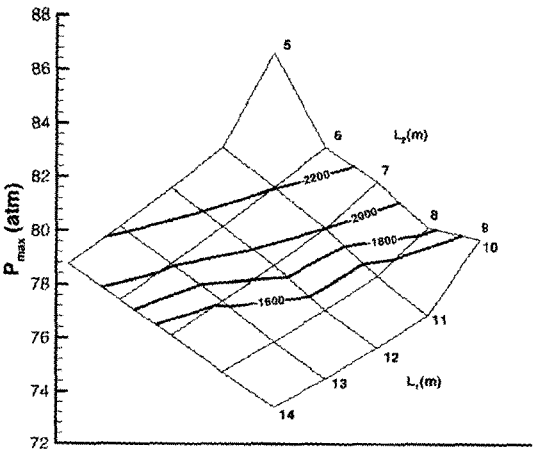

Fig. 9 Design space of SRS (P_{max} in terms of L_1 and L_2)

rate as well as the maximum pressure. Lengthening L_1, however, lowers the maximum pressure and the stop distance. From the figures, it is decided $L_1=12$ m and $L_2=8$ m as a reasonable choice. Finally, the design space survey results in terms of P_3 and L_3 are given in Figs. 10 and 11. It is interesting to note that increasing L_3 above $L_3>3$ m does not change the deceleration rate or the stop distance. It takes longer for the reflected shock to hit the bullet, as the length of the last tube gets longer. The shock hits the bullet after projectile has stopped, which makes no influence on the deceleration rate. If we use $L_3<3$ m, the reflected shock could stop the bullet eariler. As can be seen in Fig. 10, however, the deceleration rate exceeds the design limit. Figure 11 indicates that lowering P_3 will bring P_{max} down. Therefore, it is decided that the values of P_3 and L_3 are 1 and 4, respectively.

In Fig. 12(a) and 12(b), the performance of the designed small scale SRS is presented. Three peaks in the head pressure of the projectile indicate the shock impinging on the projectile, which can also be seen in the deceleration rate. However, the last pressure peak occurs after the bullet stops, which does not change the performance of the SRS. The bullet stops at 14.2 m from the muzzle breaker. The maximum pressure inside the SRS reaches at 76 atm.

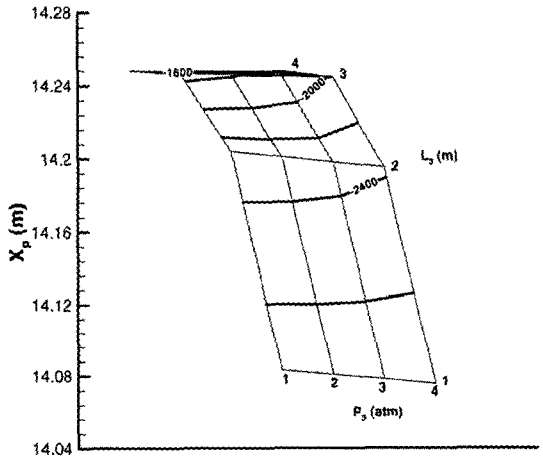

Fig. 10 Design space of SRS (X_p in terms of P_3 and L_3)

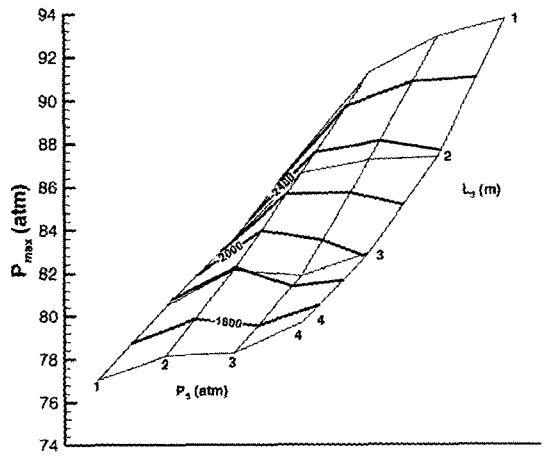

Fig. 11 Design space of SRS (X_{max} in terms of P_3 and L_3)

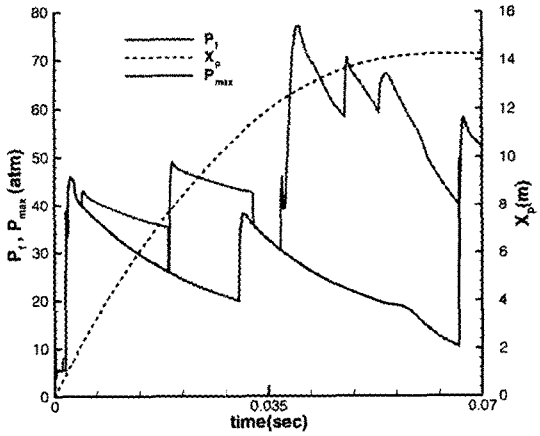

(a) Time Histories of P_f, P_{max}, and X_p

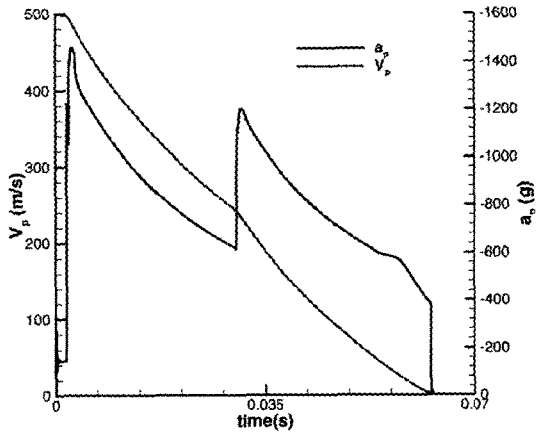

(b) Time Histories of P_{max} and a_p

Fig. 12 Performance results of designed SRS

5. Concluding Remarks

A new performance analysis code for the SRS based on the ballistic compression decelerator concept has been developed. The code is based on the one-dimensional compressible Euler code on deformable grid system and the projectile motion analysis code. The flow analysis part of the code has been verified against the exact solutions of three verification problems: the moving piston problem, the shock reflection problem and Sod's problem. A small scale SRS has designed with the requirement that it can stop safely a 20 mm bullet fired at 500 m/s within the deceleration limit of 1,600 g. The SRS consists of three tubes of which initial tube pressures are 8, 15 and 1 atm, respectively. The total length of the SRS is 25 m including a 1 m atmospheric tube that is attached to the gun barrel. The maximum deceleration rate is less than 1,470 g and the maximum pressure inside the SRS is 76 atm.

Acknowledgements

This research was supported by Agency for Defense Development via HEMRC (High Energy Material Research Center), Inha University. Their financial supports are gratefully acknowledged.

References

Baysal, O., 1986, "Navier-Stokes Analysis of Muzzle-Blast-Type Waves," *AIAA Journal*, Vol. 24, No. 5, pp. 800~806.

Clarke, E. V., Ruth, C. R., Evans, J. W., Bowen, J. E. and Hewitt, J. R., 1981, *Large Caliber Projectile Soft Recovery*, Memorandum Report ARBRL-MR-03083.

Evans, J. W., Ruth, C. R. and Clarke, E. V., 1981, *Soft Recovery Tests of A 1500-mm Cannon Launched Guided Projectile Warhead*, Type T, Memorandum Report ARBRL-MR-03107.

Grossman, B. and Walters, R. W., 1989, "Analysis of Flux-Split Algorithms for Euler's Equation with Real Gases," *AIAA Journal*, Vol. 27, No. 5, pp. 524~531.

Harten, A., 1983, "High Resolution Schemes for Hyperbolic Conservation Laws," *J. of Comp. Physics*, Vol. 49, pp. 357~393.

Hölzle, J., 2001, "Soft Recovery of Large Caliber Flying Processors," *19th International Symposium of Ballistics*, Interlaken, Switzerland.

Merkle, C. L. and Athavale, M., 1987, "Time-Accurate Unsteady Incompressible Flow Algorithms Based on Artificial Compressibility," *AIAA paper 87-1137, Proceedings of AIAA 8th Computational Fluid Dynamics Conference*, Honolulu, Hawaii.

Sod, G. A., 1978, "A Survey of Several Finite Difference Methods for Systems of Nonlinear Hyperbolic Conservation Laws," *J. of Comp. Physics*, Vol. 27, pp. 1~31.

Teng, R. N., 1972, *Ballistic Compression Decelerator*, U.S. Patent No. 3, 678, 745, issued to McDonnell Douglas Corporation.

Thomas, P. D. and Lombard, C. K., 1978, "The Geometric Conservation Law-A Link Between Finite-Difference and Finite-Volume Methods of Flow Computation on Moving Grids," *AIAA paper 78-1208, AIAA 11th Fluid and Plasma Dynamics Conference*, Seattle, Washington.

Van Leer, B., 1979, "Towards the Ultimate Conservative Difference Scheme. V. A Second Order Sequel to Godunov's Method," *J. of Comp. Physics*, Vol. 32, pp. 101~136.